Thesis for the Degree of Master

A study on CP violation in the $D^0 \to \pi^+\pi^-$ and $D^0 \to K^+K^-$ decay channels using the Belle II experiment and a detailed research on the $D^{*+} \to D^0\pi^+$ decays to develop a related analysis software tool

Belle II 실험의 D^0 중간자 붕괴 시뮬레이션을 이용한 CP 깨짐 연구와 이를 위한 D^{*+} 중간자의 붕괴를 이용한 분석 소프트웨어 개발

December 2021

Department of Physics

Graduate School of Soongsil University

Ijeong Na

Thesis for the Degree of Master

A study on CP violation in the $D^0 \to \pi^+\pi^-$ and $D^0 \to K^+K^-$ decay channels using the Belle II experiment and a detailed research on the $D^{*+} \to D^0\pi^+$ decays to develop a related analysis software tool

Belle II 실험의 D^0 중간자 붕괴 시뮬레이션을 이용한 CP 깨짐 연구와 이를 위한 D^{*+} 중간자의 붕괴를 이용한 분석 소프트웨어 개발

December 2021

Department of Physics

Graduate School of Soongsil University

Ijeong Na

Thesis for the Degree of Master

A study on CP violation in the $D^0 \to \pi^+\pi^-$ and $D^0 \to K^+K^-$ decay channels using the Belle II experiment and a detailed research on the $D^{*+} \to D^0\pi^+$ decays to develop a related analysis software tool

A thesis supervisor : Doris Y Kim

Thesis submitted in partial fulfillment of the requirements for the Degree of Master

December 2021

Department of Physics

Graduate School of Soongsil University

Ijeong Na

To approve the submitted thesis for the

Degree of Master by Ijeong Na.

Thesis Committee

Chair	이 태 훈	(signature)
Member	천 명 기	(signature)
Member	김 양 수	(signature)

December 2021

Graduate School of Soongsil University

ACKNOWLEDGEMENTS

가장 먼저, 많은 일들을 맡고 계신 중에도 저를 지도해주신 김양수 교수님께 감사드립니다. 석사과정을 시작한 순간부터 시뮬레이션 소프트웨어 코드, 클러스터 관리는 물론 데이터 분석까지 제가 관심을 가진 모든 것들에 기회를 열어주신 덕분에 지난 석사 2년이 진심으로 즐거웠습니다. 전부 처음 하는 일들이었던지라, 지금 되돌아보면 불필요했을지도 모를 시행착오를 많이 겪었고 때때로 본분인 연구보다 더 많은 시간을 쓰기도 했음에도 계속 시도할 수 있도록 격려해 주셨기에 석사 과정의 모든 성과를 수 있었습니다. 분석에 있어서는 여전히 완성되지 않은 부분이 많고, 연구가 어느정도 진행된 후에야 스스로 부족한 점이 눈에 보이기 시작한 만큼 앞으로 갈 길이 멀지만 교수님께 배운 것들을 기억하며 꾸준히 성장해 나가도록 노력하겠습니다.

미팅에서 끊임없이 연구 방향을 바로잡아 주신 BelleII Charm group의 Giulia Casarosa, Longke Li,Alan Schwarz 그리고 Angelo Di Canto 교수님들께도 감사드립니다. 첫 번째 발표에서부터 지금까지 이루어진 연구의 거의 모든 내용은 교수님들의 코멘트가 있었기에 가능했습니다. 그리고 Charm skim liason 으로써 Data production 에 도움을 주신 Emma Oxford와 Guanda Gong 선생님들께도 감사의 인사를 올립니다.

논문 심사위원을 맡아 주신 두 분의 교수님께도 감사의 인사를 올립니다. 먼

저 이태훈 교수님, 학부와 양자역학 4과목과 입자물리학 수업까지 교수님께서 강의해 주셨기에 항상 흥미를 가지고 집중할 수 있었습니다. 그리고 천명기 교수님, 1학년 일반물리 수업부터 4학년 졸업논문까지 모자란 모습만 보여드린 것 같아 항상 죄송하고 아쉬웠습니다. 부족한 논문임에도 교수님께 평가를 맡길 수 있음은 제게 큰 영광입니다. 또한 천명기 교수님 연구실의 양 박사님께도 감사의 인사를 드립니다. 짧은 시간이었지만 박사님께서 가르쳐 주신 것들은 지금까지 연구를 하는 데 큰 힘이 되고 있습니다.

또한 많이 부족했던 학부생에게 연구과정에 참여할 기회를 주신 이윤상 교수님과, 컴퓨터 물리 분석을 시작하게 해 주신 김창배 교수님, 연구에 성실하게 임하도록 격려해 주신 이동렬 교수님 그리고 실험조교 내내 함께해 주신 최현희 교수님께도 큰 감사를 드립니다. 학부 4년과 석사 2년을 통틀어, 어려울 때마다 항상 교수님들께서 조언해 주셨기에 무사히 석사과정까지 마칠 수 있었습니다. 석사과정 동기들과 김재연 선배, 그리고 328호실의 두 선배들에게도 감사드립니다. 전부 전공이 달랐지만 그렇기에 함께 공부하는 것이 더 즐거웠습니다.

그리고, 가장 중요한, 가족들과 언니, 그리고 이모들, 항상 곁에 계셔 주심에 감사드립니다.

TABLE OF CONTENTS

ABSTRACT IN KOREAN vi

ABSTRACT IN ENGLISH vii

CHAPTER 1 Introduction 1

1.1 Charge-Parity violation in neutral D meson decay 1

1.2 Experimental Method 2

CHAPTER 2 Experimental Setup 5

2.1 SuperKEKB 5

2.2 BelleII Detector 6

2.2.1 Vertex Detector 9

2.2.2 Central Drift Chamber 10

2.2.3 PID system 11

2.2.4 Electromagnetic Caloriemeter 13

2.2.5 KLM 14

2.3 Simulation 15

2.3.1 BelleII VR 16

2.4 Computing 17

2.5 BelleII Analysis Software Framework 19

CHAPTER 3 Event Selection 21

3.1 Dataset 21
3.1.1 Note on the dataset 21
3.2 Preselection and Reconstruction 22
3.3 Refining Selection Criteria 26
3.3.1 BinaryPID 26
3.3.2 Selection of Signal Window 27
3.4 Yield Fit 30

CHAPTER 4 ACP Measurement 35

4.1 D^0 raw asymmetry distribution 35
4.2 Raw Asymmetry and Slow Pion 36
4.3 Linear fit of A_{CP} 41
4.4 Systematic 42

CHAPTER 5 Conclusion 44

References 46

LIST OF TABLES

[Table 3-1] Preselection criteria at the reconstruction process . . . 22

[Table 3-2] Total number of entries in analysis box and purity in signal region, Here, signal window size is 0.036 GeV and 0.0036 GeV for mass and ΔM 23

[Table 3-3] Minimum estimated asymmetry regarding the width of signal window 30

[Table 3-4] Fit result 32

[Table 5-1] Result 44

LIST OF FIGURES

[Figure 2-1] Schematic Overview of SuperKEKB accelerator[6] . . 5

[Figure 2-2] Schematic view of nanobeam scheme[9]. Small beam bunches collides at the IP with a large crossing angle, which results in minimizing the size of overlap region. 6

[Figure 2-3] Top view of BelleII detector 8

[Figure 2-4] cross-sectional view of vxd detector[10] 10

[Figure 2-5] Wire configuration of Belle and BelleII[13] 11

[Figure 2-6] Working principle of ARICH[15] 13

[Figure 2-7] Working principle of iTOP[16] 13

[Figure 2-8] Simulation screen from [22] 16

[Figure 2-9] Concept of BelleII computing model, from [24] 17

[Figure 2-10] Summary of the categories and tasks of computing sites, from [24] 18

[Figure 3-1] Mass distribution of untagged decay. 24

[Figure 3-2] Reconstructed mass and distribution 25

[Figure 3-3] FoM with respect to the binaryPID selection criteria . . 28

[Figure 3-4] efficiency with respect to the binaryPID selection criteria 29

[Figure 3-5] Estimated asymmetry regarding the width of signal window. The selection criteria in Cabibbo favored channel should be consistent Thus the mass window of $D^0 \to K^-\pi^+$ is optimized the quadratic of their error[4] . . . 31

[Figure 3-6] Fit result of Untagged D^0 to $\pi^+\pi^-$ fit result 33

[Figure 3-7] Fit result of Tagged D^0 to $\pi^+\pi^-$ fit result. log scale plots are also shown in the top right in the each plots. 34

[Figure 4-1] The raw asymmetry of D^0 along $\cos\theta$ 35

[Figure 4-2] The raw asymmetry of D^0 along p 36

[Figure 4-3] slow pion transverse momentum distribution and asymmetry p 37

[Figure 4-4] A_{raw}^{untag} (above) and corresponding statistical error (below) 39

[Figure 4-5] A_{ϵ}^{π} (above) and statistical error (below) 40

[Figure 4-6] A_{CP}^{KK} (left) and statistical A_{FB}^{KK} (right) 42

[Figure 4-7] $A_{CP}^{\pi\pi}$ (left) and statistical $A_{FB}^{\pi\pi}$ (right) 43

국 문 초 록

Belle II 실험의 D^0 중간자 붕괴 시뮬레이션을 이용한 CP 깨짐 연구와 이를 위한 D^{*+} 중간자의 붕괴를 이용한 분석 소프트웨어 개발

나이정

물리학과

숭실대학교 대학원

2019년 시작된 벨 2 실험은 2021년 7월까지 123.17/fb에 이르는 데이터를 수집했고, 이에 따른 시뮬레이션 데이터 또한 1/ab에 다다랐다. 이 논문은 벨 2 실험의 시뮬레이션 데이터로 D^0 중간자가 전하가 반대인 두 하드론으로 붕괴하는 과정의 전하-반전성 비대칭 정도를 계산하는 것을 목적으로 하며, 이를 위해 D^0 붕괴 모드 연구에서 널리 쓰여 온 방법인 D^{*+} 태그 방법을 바탕으로 한 ROOT기반의 물리 분석 코드를 짜고, 이 도구를 시뮬레이션 데이터에 적용하여 예비 결과를 얻으며 이로써 시뮬레이션에서 얻은 모델을 차후 충돌 데이터 분석에 활용할 가능성을 모색한다.

ABSTRACT

A study on CP violation in the $D^0 \to \pi^+\pi^-$ and $D^0 \to K^+K^-$ decay channels using the Belle II experiment and a detailed research on the $D^{*+} \to D^0\pi^+$ decays to develop a related analysis software tool

Ijeong Na
Department of Physics
Graduate School of Soongsil University

The Belle II experiment started its physics run in 2019 and has accumulated more than 213.49/fb heretofore, and aims to accumulate more than 50/ab until the end of the experiment. Based on the latest BelleII Monte Carlo simulation dataset, this thesis delve into the strategy to search for CP violation effect in the $D^0 \to \pi^+\pi^-$ and $D^0 \to K^+K^-$ channels in order to perform the real data analysis by adopting the D^{*+} tagging method which have been used from Belle experiment. The event selection and fitting procedures to obtain the preliminary result will be discussed, while thoroughly investigating the accuracy and usability of the D^{*+} tagging method.

CHAPTER 1 Introduction

1.1 Charge-Parity violation in neutral D meson decay

The combined transformation of charge conjugation and parity is violated only in weak interactions by the irreducible complex phase in the CKM matrix [1]. There are three types of CPV −(1) Direct CP violation, also referred to as the CPV in decay, where the decay amplitude of a process and its CP conjugate process are not equal; (2) Indirect CP violation, also known as CPV in mixing, which occurs when the two weak eigenstates are not mass eigenstates; (3) CPV in interference between mixing and decay.

Under the standard model, the amount of CP violation in singly Cabibbo suppressed(SCS) decay is expected to be negligible being on the order of 10^{-3} 10^{-4}. However, prediction of the amount of CPV is difficult due to the perturbative QCD effect at low energies [1, 2] hence the high-precision measurement is needed to verify the Standard Model(SM), while also being vitally sensitive to new physics beyond the SM. The time-integrated CP asymmetry in $D^0 \to K^-K^+$ and $D^0 \to \pi^-\pi^+$ have been studied in BaBar[3], Belle[4] and LHCb[5]. In these channels the direct contribution in the asymmetries are expected to have same magnitude but opposite signs, the difference in CP asymmetries, ΔA_{CP} is very sensitive to the direct CPV measurement. The latest result was observed

from LHCb, $\Delta A_{CP} = (-15.4 \pm 2.9) \times 10^{-4}$ which was the first observation of non-zero direct CP violation. Accordingly, this thesis aims to build a analysis model adopting the D-star tagging method which was used in previous analysis on Belle[4], in order to open the BelleII collision data analysis which aims to be 50/ab.

1.2 Experimental Method

The time-integrated CP asymmetry in D^0 two-body decay can be described in terms of the asymmetry of time-integrated decay rates, where h denotes the hadron (kaon or pion.)

$$a_f = \frac{\Gamma(D^0 \to h^+h^-) - \Gamma(\overline{D^0} \to h^+h^-)}{\Gamma(D^0 \to h^+h^-) - \Gamma(\overline{D^0} \to h^+h^-)} \tag{1.1}$$

Assuming that the total decay widths of a particle and its antiparticle are equal, 1.1 can be re-written in the asymmetry of the number of reconstructed D^0 and $\overline{D^0}$ mesons, as expressed in the first line of Equation 1.2. The flavor of D^0 from the $D^{*+} \to D^0\pi_s^+$ decay is determined by slow pion's charge. In other words, D^0 is tagged with the slow pion's charge at the production. The asymmetry of the reconstructed D meson can be factorized into several components, as shown

in the second line of Equation 1.2.

$$\begin{aligned} A^{reco} &= \frac{N(D^0 \to h^+h^-) - N(\overline{D}^0 \to h^+h^-)}{N(D^0 \to h^+h^-) + N(\overline{D}^0 \to h^+h^-)} \\ &= A_{FB}^{D^{*+}} + A_{CP}^{hh} + A_{\epsilon}^{\pi} \end{aligned} \tag{1.2}$$

Here, A_{ϵ}^{π} represents the slow pion detection asymmetry caused by the charge-dependent material response. $A_{FB}^{D^{*+}}$ denotes the production asymmetry of D^{*+}, which is an odd function in the polar angle bin in the center-of-mass(CMS) frame. Thus, if A_{ϵ}^{π} is known, one can correct the reconstruction asymmetry as in Equation 1.3.

$$A_{corr}^{reco}(\cos\theta^*) = A_{FB}^{D^{*+}}(\cos\theta^*) + A_{CP}^{hh} \tag{1.3}$$

A_{CP} and the D^{*+} production asymmetry are then separated by adding and subtracting the opposite bins of $\cos\theta^*$.

$$\begin{aligned} A_{CP}^{hh} &= \frac{A_{cor}^{rec}(\cos\theta^*) + A_{cor}^{rec}(\cos\theta^*)}{2} \\ A_{FB}^{hh} &= \frac{A_{cor}^{rec}(\cos\theta^*) - A_{cor}^{rec}(\cos\theta^*)}{2} \end{aligned} \tag{1.4}$$

A_ϵ^π is calculated from the Cabibbo-favored channel, $D^0 \to K^-\pi^+$ as the reference mode.

$$\begin{aligned} A_{tag} &= A_{FB} + A_{CP}^{K\pi} + A_\epsilon^{K\pi} + A_\epsilon^\pi \\ A_{utg} &= A_{FB} + A_{CP}^{K\pi} + A_\epsilon^{K\pi} \\ A_\epsilon^\pi &= A_{tag} - A_{untag} \end{aligned} \tag{1.5}$$

If the production asymmetry of D^{*+} is equal in both tagged decay and untagged decay, the only difference in the asymmetry will arise in slow pion detection efficiency when the selection criteria for the final-state hadrons are the same for both tagged and untagged channels.

CHAPTER 2 Experimental Setup

2.1 SuperKEKB

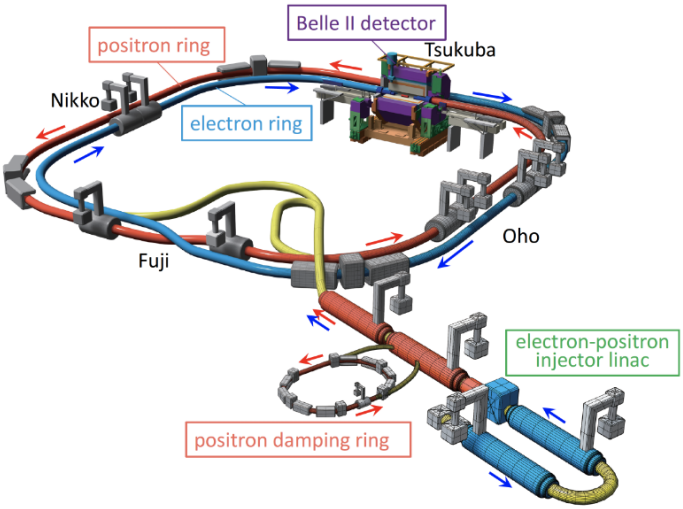

[Figure 2-1] Schematic Overview of SuperKEKB accelerator[6]

SuperKEKB is an asymmetric e+e- collider located in Tsukuba, Japan, constructed by upgrading the KEKB. The electron and positron bunches are accelerated to the opposite direction with asymmetric beam energy - 4.0GeV for positrons and 7.007 GeV for electrons, corresponding to Upsilon 4s resonance (10.58 GeV). These two bunches intersect in the interaction point(IP), and the luminosity at this point is defined as below :

$$\mathscr{L} = \frac{2er_e}{\gamma_{e^\pm}}\left(1+\frac{\sigma_y^*}{\sigma_x^*}\right)\left(\frac{I_{e^\pm}\times\xi_{y,e^\pm}}{\beta_y^*}\right)\left(\frac{R_L}{R_{\xi_y}}\right) \tag{2.1}$$

It is, higher beam current, larger beam-beam tune-shift parameters $\xi_{y,e^{\pm}}$ and smaller vertical beta function β_y^* at the interaction point(IP) is required to achieve high luminosity. Compared to KEKB, SuperKEKB has doubled beam current and reduced β_y^* while $\xi_{y,e^{\pm}}$ remains as same as KEKB by squeezing the beams up to 50 nm, 6 micrometers in each x and y-direction. This was implemented by the "nano-beam"scheme, which was originally proposed at the Italian SuperB project[7]. The design value of its peak luminosity is of $8 \times 10^{35} cm^{-2} s^{-1}$ and $50 ab^{-1}$ which is 40 times larger than KEKB[8].

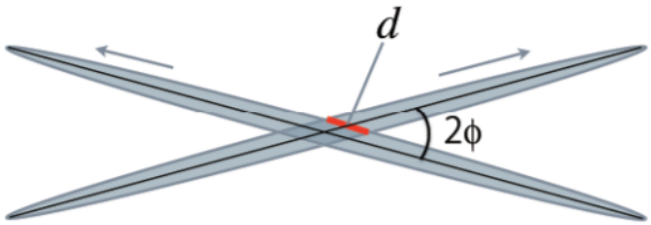

[Figure 2-2] Schematic view of nanobeam scheme[9]. Small beam bunches collides at the IP with a large crossing angle, which results in minimizing the size of overlap region.

2.2 BelleII Detector

The event produced in the collision is identified by reconstruct the interaction and their final decay product. Based on the fact the detector signal is obtained from the electromagnetic interaction and radiation of charged particles, particles should live long enough, and should interact with the detector material

to be detected. Thus, only stable particles −proton, neutron, kaon, pion, electron, muons and photon can be observed in the detector. Detector measures their momentum, charge, energy, lifetime and velocity of these particles and extract the PID(Particle Identification) information. BelleII detector consists of 5 groups of subdetectors dedicated to reconstruct physics observable. The overall design of BelleII detector is partially inherited from its predecessor, Belle. However the subdetectors, readout components and computing systems were upgraded to manage higher beam induced background and radiation damage which follows as a consequent of achieving higher luminosity provided by upgraded accelerator. The overall performance and hermeticity of the spectrometer should remain at the same time[6-8]. In the New detector, the vertex detectors were newely designed - the vertex detectors and PID systems were newly designed. Some part of KLM components, ECL crystals and superconducting solenoid remains. figure 2-3 illustrates the top view of the BelleII detector. It hasvasymmetric shape along the z axis because the produced frame from the collision heads to the forward direction. In the following selection. Detector can be separated in three region by polar angle ranges. Forward region covers 17 to 30 in polar angle.[9, 10]

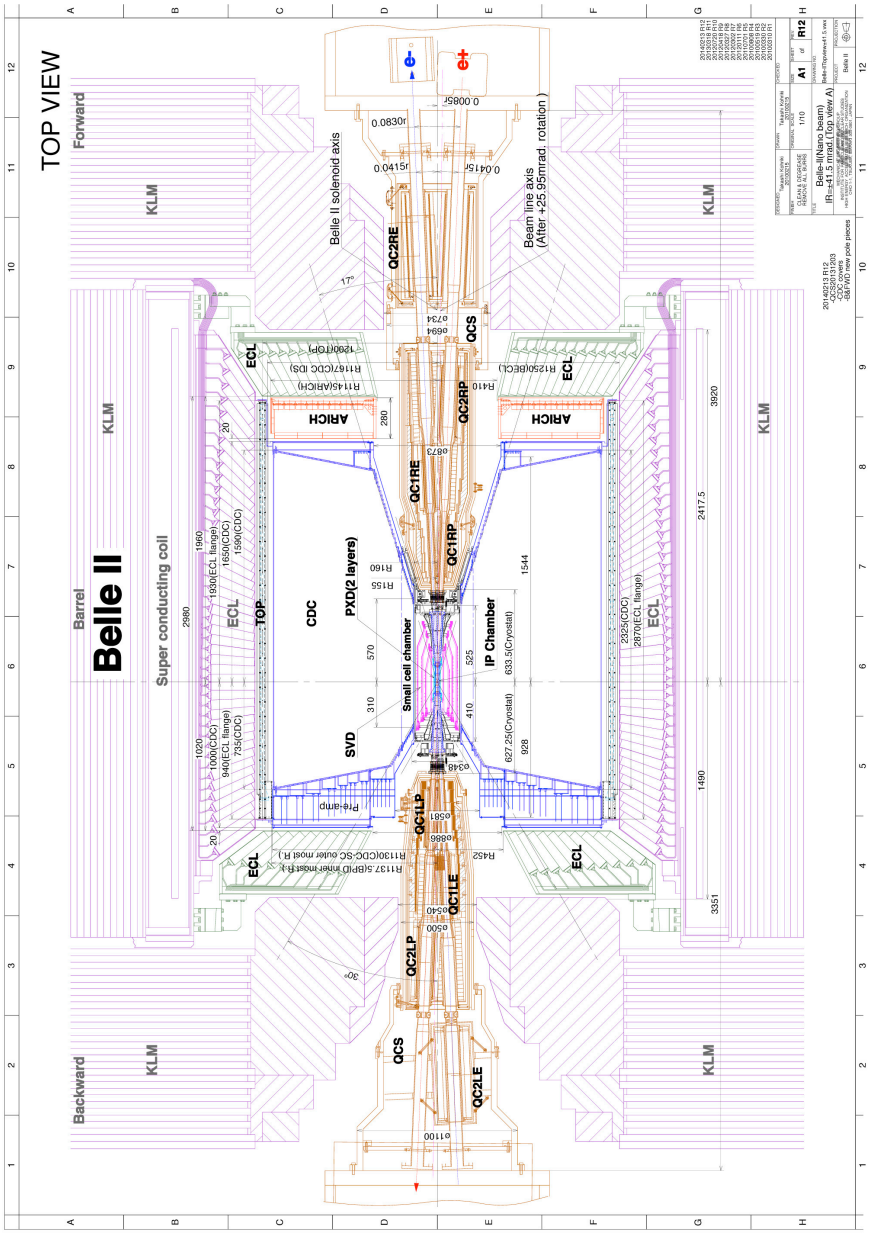

[Figure 2-3] Top view of BelleII detector

2.2.1 Vertex Detector

Asymmetric beam energy allows to measure the flight distance, thus enables the time dependent CPV analysis by measuring decay time measurement of short-living particles such as B and D mesons. Thus, reconstructing the vertices of these short-living particles plays a huge role in the physics goal. The Vertex Detector (VXD) is located at the innermost layer of the Belle2 detector. Two layers of PiXel Detector(PXD) are installed in close proximity, where two layers are located at 14mm and 22mm from the IP. Four layers of Silicon Vertex Detector(SVD) are located outer. The cross-sectional view is illustrated in figure 2-4.

PXD comprises 8 million pixels and functions based on the depleted p-channel field-effect transistor(DEPFET) technology[11]. Each pixel is a p-channel FET on a completely depleted silicon bulk. When the particle leaves electrons and holes while passing through the detector, the hole moves backward, and charges are collected at the internal gate. To avoid the screening effect of this accumulated charge, a positive pulse-form voltage is applied to a clear contact[11]. Thus the DEPFET sensors can simultaneously detect and amplify the signal. SVD is made of double-sided silicon straps. P-side strips are parallel to the beam while n-side straps are placed perpendicular to the beam direction. These strips

provide r-phi and z information of a track. SVD extrapolates the track information to the PXD, reconstructs tracks from hits, and provides standalone tracking.[12]

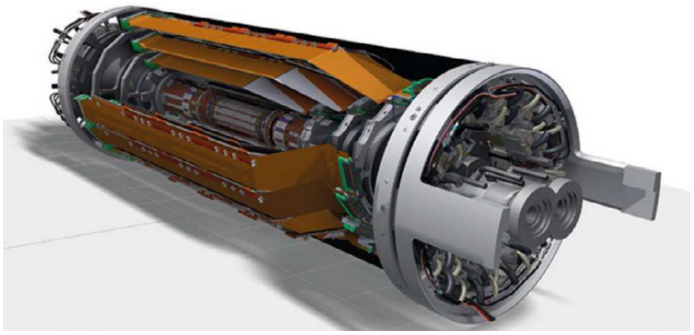

[Figure 2-4] cross-sectional view of vxd detector[10]

2.2.2 Central Drift Chamber

Central Drift Chamber (CDC) is the main tracker responsible for momentum measurement, tracking, providing trigger signal, and particle identification[9]. It is a cylindrical shape and has nine super layers, 56 layers, and 14336 wires. The chamber is filled with a gas mixture of 50% helium and 50% ethane. When a charged particle passes through the detector, the gas particles are ionized along the track and produce primary electrons. These electrons drift to the anode wires and generate secondary electrons, which create avalanches. A high voltage is applied to the field wires to generate an electric field, which is required to accelerate the electrons. A hit is generated when the electron reaches the sense wire,

and the wire measures the drift time. CDC measures momentum from deflection within a magnetic field by reconstructing these hits. Figure 2-5 illustrates the wire configuration inside the CDC chamber. As shown in the figure, the cell size was decreased during the upgrade to handle the large beam background by reducing the hit rate per wire.[13]

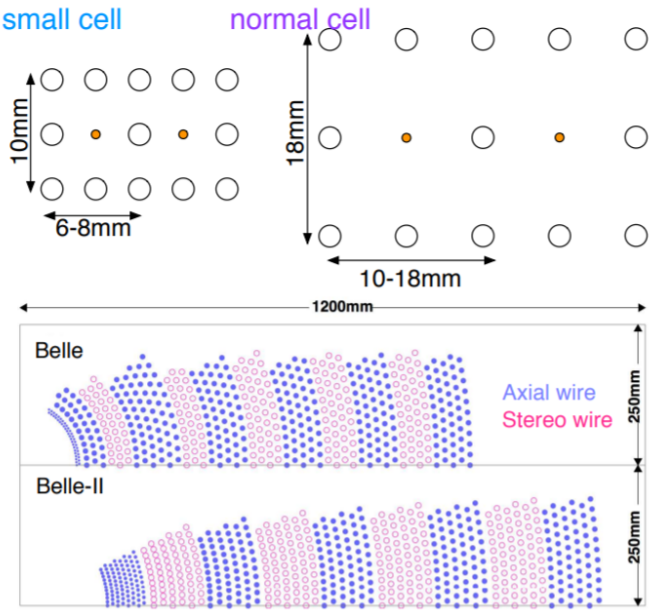

[Figure 2-5] Wire configuration of Belle and BelleII[13]

2.2.3 PID system

The PID determines the particle species, which is basically to estimate the mass of a particle which can be calculated from combined information on observables such as velocity, total energy, and penetration depth with momentum. In BelleII, a PID is described by the ratio of likelihoods. Thus, for example, a

pion's global PID is defined as Equation 2.2.

$$\frac{\mathscr{L}_{\pi}}{\mathscr{L}_{\pi} + \mathscr{L}_{K} + \mathscr{L}_{\mu} + \mathscr{L}_{p} + \mathscr{L}_{n} + \mathscr{L}_{d}} \tag{2.2}$$

Each detector component uses various strategies to construct this likelihood ratio. For example, the SVD and CDC use dE/dx to distinguish among charged particle hypotheses with known momenta, the ECL uses the shape of electromagnetic showers, and the KLM uses hadronic showers to identify K-Long mesons[14]. Together with this information, PID dedicated detector aims to distinguish the species of the charged particles with high separation efficiency, especially for kaons and pions. In BelleII, PID system consists of two Cherenkov subdetectors - an imaging Time Of Propagation counter (iTOP) in the barrel region and an Aerogel Ring Imaging Cherenkov(ARICH) in the forward endcap region. ARICH is proximity focusing RICH which employed two layers of aerogel with different reflective indices as a Cherenkov radiator. Thus, emitted Cherenkov photons are overlapped on the photon detector. The working principle is shown in 2-6. iTOP detector measures the velocity of a particle by measuring the time of flight. The charged particle emits the Cherenkov radiation while they passing through the quartz radiator. These photons are internally reflected towards the end of the bar, where sensors are located. Operating principle is illustrated in Figure 2-7. Thus, the detector distinguishes kaons from pions based

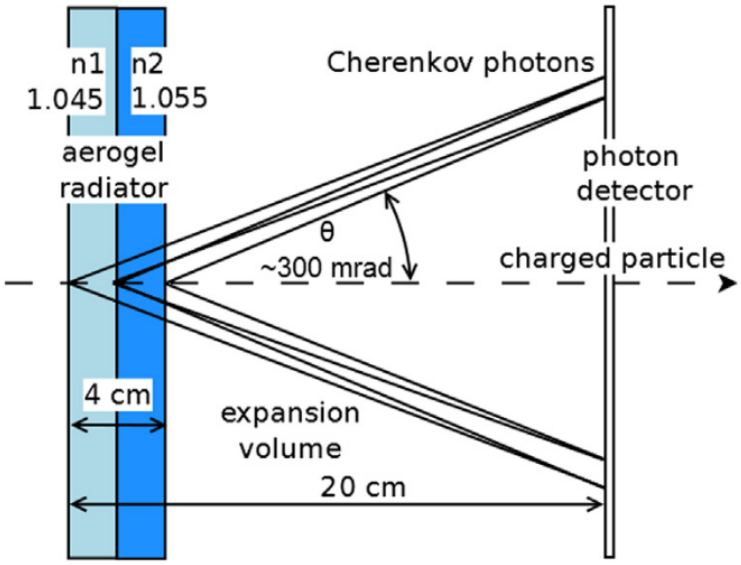

[Figure 2-6] Working principle of ARICH[15]

on the different arrival times and the locations of the emitted photons.[16]

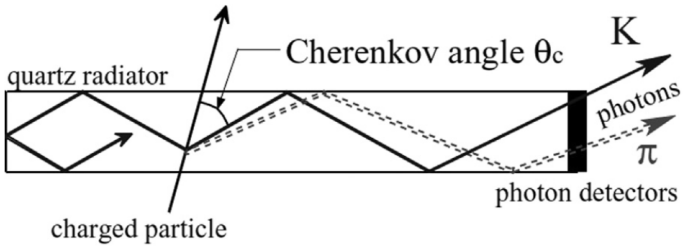

[Figure 2-7] Working principle of iTOP[16]

2.2.4 Electromagnetic Caloriemeter

Neutral particles such as pi^0 and photons do not interact with the CDC or the tracking devices. However, they deposit energy in the calorimeter and produce a shower until they are fully absorbed. Belle II has an ECL that determines

the energies and spatial coordinates of these neutral particles. The main function of ECL is to detect the energy and angular coordinates of photons with high efficiency. It also provides information for election identification and K-long detection, generates trigger signal of proper signal for a trigger and measures luminosity measurement[9]. ECL measures the electromagnetic energy of a particle based on the shower shape. From the composition and dimensions of this shower type, the primary particle's energy can be determined. ECL also provides PID information from the different material responses by the particle. During the upgrade, the 8736 CsI(Ti) scintillator crystals were reused from the Belle detector, but readout electronics were improved to handle pile-up noise and fake clusters from high-energy photons.[17]

2.2.5 KLM

The KLM detector is located at the outermost part of the detector and is composed of thin active layers interspersed with iron plates. These iron plates return the magnetic flux of the 1.5T solenoid. The primary function of KLM is to separate neutral hadrons from muons. The relatively high penetrating power of muons allows them to pass through the detector without leaving a shower. On the other hand, neutral hadrons such as K_L^0 produce a hadronic shower since they interact with detector material hadronically. [18]

2.3 Simulation

The analysis is performed on ”generic Monte Carlo (MC)” data, including background processes. This data is generated from full detector simulation. In BelleII, MC production is managed in centrally as in a project. In general, the MC production campaign follows the major upgrade schedule of the major upgrade of the software package. The resulting data is saved in the same format as the real data, i.e mDST. The purpose of the simulation is to create a model to study the actual data, considering our expectations based on the given information[19] In this regard, the simulated event should mimic the natural phenomena, and the interaction between the resulting particles and the detector material should mimic that in the real detector. The BelleII MC production follows several steps. First, MC particles are generated using the event generators such as EvtGen and Pythia. Then, the Geant4[20] toolkit, a C++ library, simulate the detector response by tracking each particle over time. Unit of this process is called ’step’ and stored in the G4Step object. The object stores the list of step points, particleID, terminant time and energy loss and updates every time point where the physics process is invoked. The secondary particles generated during the decay or interaction are also stored in the particle list and tracked. Physics processes involved here are implemented in PhysicsList class, which consists of information on every parti-

cle involved in the physics process and the corresponding production thresholds. The belle2 analysis toolkit provides two options for this. One is the FTFP_BERT, which is commonly used in high-energy physics applications. It used to be the default physicslist in the basf2 package. The other one is Belle2PhysicsList, which has been independently developed to fulfill the requirements for the BelleII experiment. Compared to the FTFP_BERT, Belle2PhysicsList adopted a faster electromagnetic process constructor and more tuned energy range of hadronic process constructor to match the BelleII envoronment.[21]

2.3.1 BelleII VR

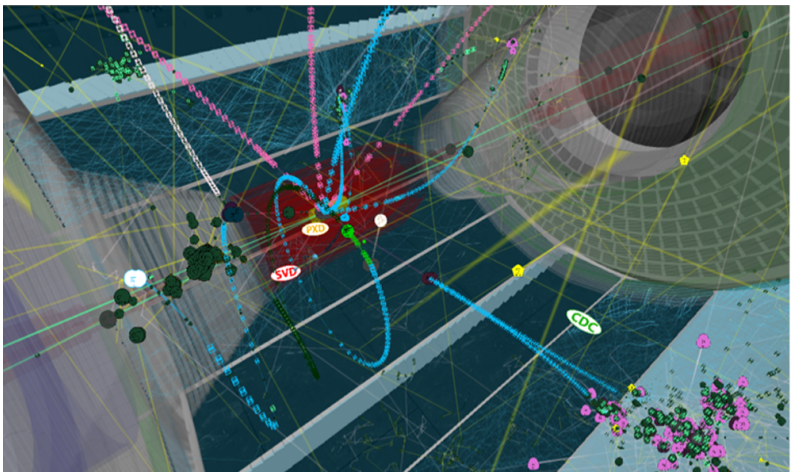

[Figure 2-8] Simulation screen from [22]

There is a toolkit that visualizes the whole BelleII detector simulation in virtual reality: Bell2VR. Based on the Unity engine, detector Geometry is defined as Filmbox(FBX), and the simulation result is invoked in each step and visualized

on the screen. Detailed information of the process is described in [23].

2.4 Computing

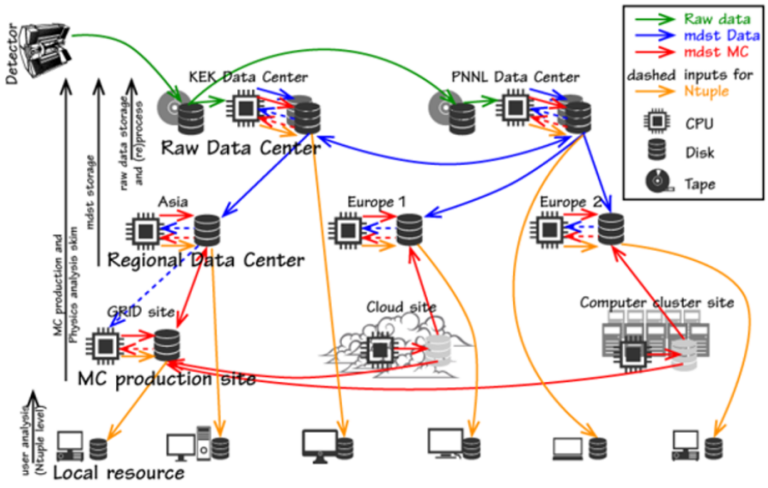

[Figure 2-9] Concept of BelleII computing model, from [24]

To process the extreme amount of beam data and MC events which corresponds to a few hundred petabytes , BelleII adopted a grid base distributed computing model[24] . The computing cites are classified into three groups as in 2-10 ; (1) Main center which has responsibility of raw data processing, MC production and user analysis. (2) Grid cites are in charge of the user analysis and MC production and (3) Non-grid cites - local resources such as personal laptop. Based on this classification, Figure 2-9 illustrates the concept of BelleII computing.

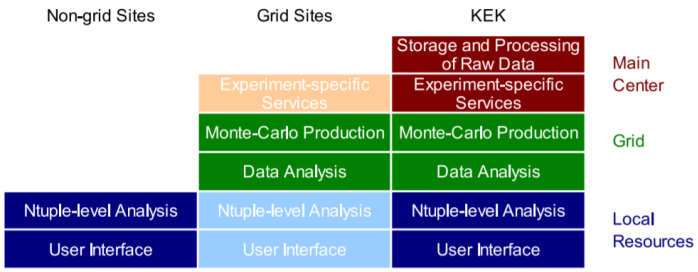

[Figure 2-10] Summary of the categories and tasks of computing sites, from [24]

Raw data from the detector is stored and processed in the KEK[1]. KEK is responsible for data acquisition and raw data processing. The output is saved as mDST object and distributed to the grid sites. One copy of raw data is transferred to PNNL and processed to lessen the heavy workload on KEK. KEK and PNNL distribute the reprocessed mDST to the BelleII grid sites. The grid cite handles user analysis from the skimmed dataset. Its framework, DIRAC[25] enables and manages the interaction between distributed resources and central computing systems. BelleII specific API and tools are provided with an extension module called BelleDIRAC, for remote job submission and data management. [26]

Along with raw data processing, Monte Carlo samples at least six times larger than the beam data are required to produced for precision measurements[27]. The resulting MC event outputs are saved in mDST format, and are placed on the disks at the grid site where they were produced. At least one replica is distributed to the other grid sites at this stage. Currently, the MC production takes place on

[1] KEK computing system is called KEK Central Computing System, KEKCC

grid sites and the cloud service as adjunct, since the MC production can be distributed easily to the grid sites since it does not require heavy input.[24, 28]

2.5 BelleII Analysis Software Framework

BelleII core software consists of tools, externals, and basf2. Tools are for the installation and configuration of externals and basf2; the external library is a collection of third-party code such as Geant4, ROOT, EventGen. The Basf2 is a collection of the Belle II specific code. Data processing, MC production, physics analysis are done on this framework. Basf2 codes are grouped in packages for subdetectors, event generation, tracking, and analysis. Each package contains modules developed in c++ codes, which is a unit of data processing. These modules can be loaded and executed in user-defined order in the steering file.[29] The physics analysis starts from writing the steering file—first, the user load data from the datastore. The ParticleList is filled with the particle array from the input mdst file. Only charged final state particles, neutral final state particles ($\gamma, K_s^0, K_l^0, \Lambda^0, e, \mu, \pi, K, p$) can be loaded in this step. Non-final state particles that can decay in a very short time (thus cannot be detected directly) are created by combining other candidates with each other by reconstructdecay, a wrapper function of the ParticleCombiner module. We can reject incorrectly combined candidates by adding a cut on the vertex fit quality. If the input data contains

MC event, one can execute MCMatching, which builds a link between particle object from track and mcparticle object, generated from event generator. If they are matched, the signal flag of this matching is set to be true, otherwise 0 or NaN.

CHAPTER 3 Event Selection

3.1 Dataset

This analysis was performed using the official Skimmed MC14ri_ax1 dataset, which is dedicated to D^0 decay from anything : XtoD0_D0ToHpJm. This corresponds to 1/ab of integrated luminosity. The data includes seven streams(ccbar, ddbar, uubar, ssbar, taupair, charged and mixed) of official Monte Carlo data. Skim includes hlt-hadron skim, which requires at least three suitable tracks with a transverse momentum larger than 0.2 and impact parameters (|d0|) < 3 and z0 < 4. It also vetoes events from Bhabha scattering. Based on this skim, the events are reconstructed with basf2 release light-2106-rhea and more selective cuts. The Tagged mode indicates the D^0 to KK, pipi, KP decay from D^{*+} , accompanying with slow pion. The charge of the slow pion determines the flavor of the D meson. The Untagged channel indicates the other D^0 s decays from anything. Both channels are reconstructed separately.

3.1.1 Note on the dataset

XtoD0_D0ToHpJm skim is usually referred as Untagged skim since it includes D^0 decays from anything. A tagged skim, DstToD0Pi_D0ToHpJm also exists; however, it was not available at the time since the Cabbibo-favored chan-

nel was omitted from the skim when moving from the MC13 to MC14 project. As the skim reproduction is now underway, tagged skim will be used for the future work.

3.2 Preselection and Reconstruction

[Table 3-1] Preselection criteria at the reconstruction process

Candidate	Selection Criteria
K, π	$\|dr\| < 1$, $\|dz\| < 3$,
	nCDCHits > 30
	$L(K,\pi)_K$ > 0.3
	$L(\pi,K)_\pi$ > 0.3
π_s	$\|d0\| < 1$, $\|z0\| < 3$
D^0	$1.81 < M < 1.91$ GeV
	$p_{CMS} > 2.5$ GeV
	pValue > 0.001
D^{*+}	0. < Q < 0.2 GeV
	pValue > 0.001

The preselection cuts are listed in 3-1. First, every charged track is required to be consistent with the interaction point(IP) since D^{*+} has a short lifetime by virtue of decaying directly via strong interaction. Two hadrons decaying from D^0 should have enough CDC hits to suppress the long tail of the D^0 mass distribution through precise momentum measurement. Additionally, the binary PID cut is

applied. Kaons and pions are easily misidentified as each other. For slow pion tracks decaying from D^{*+}, , only track cut is applied. D^0 candidates need to be in with the specified mass range and have a CMS momentum larger than 2.5 GeV. The latter cut is for rejecting D^0 decays from the $B\overline{B}$ event. For Tagged channels, D^{*+} candidates with Q values less than 0.02 are accepted. Vertex Treefit[] is also performed for each D^0 and D^{*+} vertex . For Candidates with p-values lager than 0.001 are selected, other spurious tracks are rejected. For multiple candidate decay, only one candidate with the best fit quality is accepted. The distribution of reconstructed candidates along mass and ΔM distribution are shown in Figure 3-1 and 3-2. Table 3-2 summarizes the reconstruction result inside the analysis box.

[Table 3-2] Total number of entries in analysis box and purity in signal region, Here, signal window size is 0.036 GeV and 0.0036 GeV for mass and ΔM .

Channel	Entries	Purity in signal box (%)
$D^0 \to K^-\pi^+$	415025	0.93
$D^0 \to K^+K^-$	323235	0.83
$D^0 \to \pi^+\pi^-$	3488660	0.99
Untagged $D^0 \to K^-\pi^+$	16496870	0.69

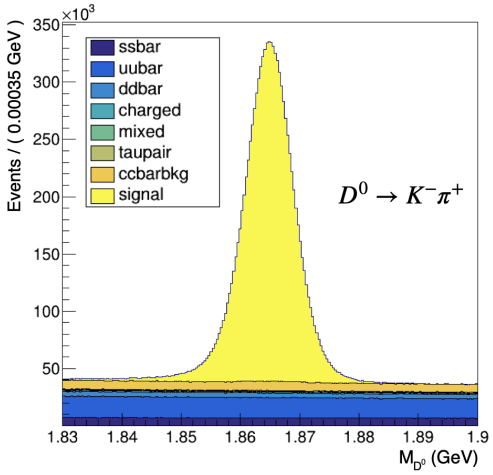

[Figure 3-1] Mass distribution of untagged decay.

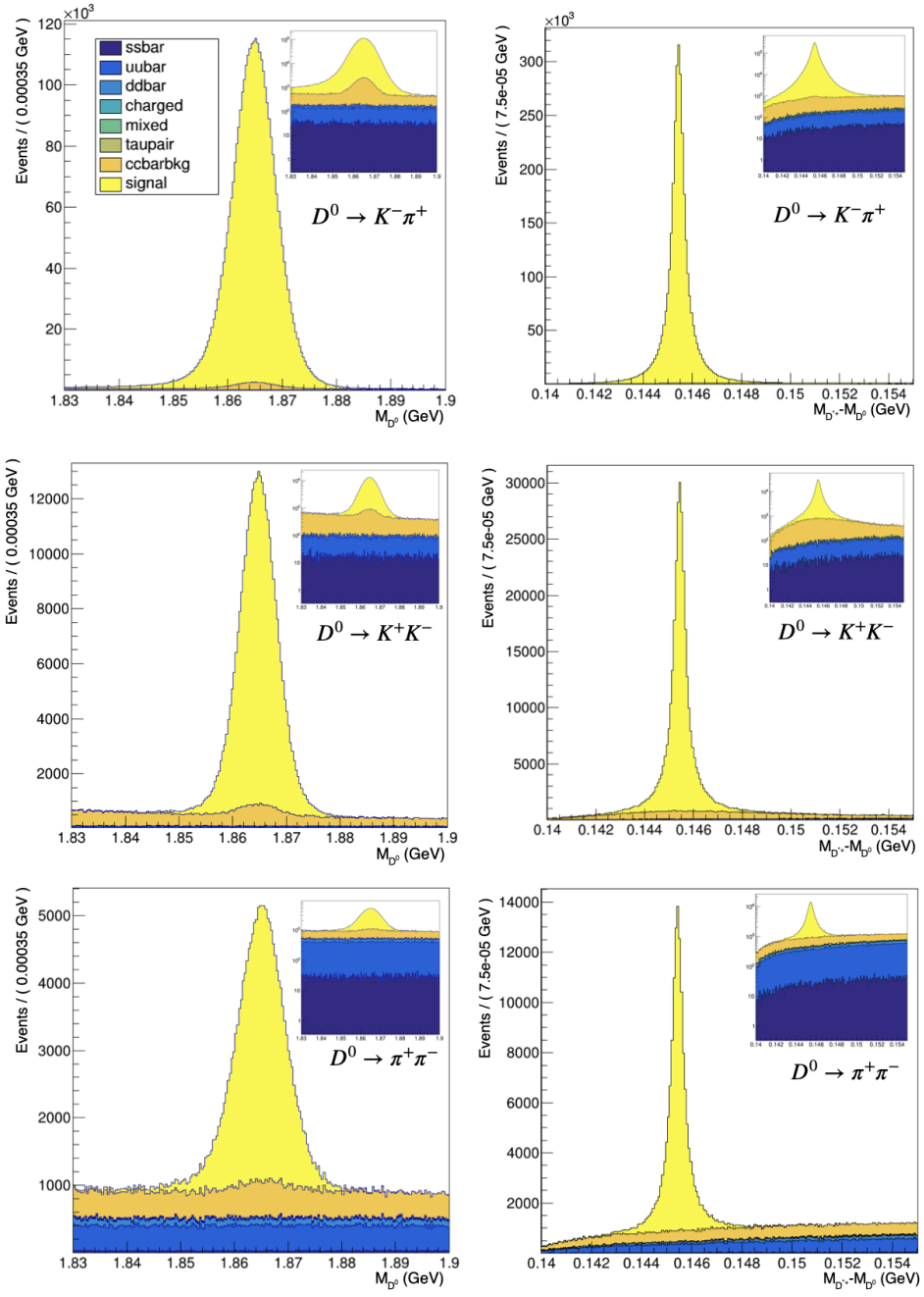

[Figure 3-2] Reconstructed mass and distribution

3.3 Refining Selection Criteria

3.3.1 BinaryPID

In the previous study, the PID selection criteria applied to the final-state hadrons was more selective than our cut. The PID cut can suppress the background from misidentified particles −when either of the kaon or pion decay from D^0 is misidentified as the each other. The impact of PID cut was studied with the efficiency (Equation 3.2) and figure of merit(3.1) along the kaon's binaryPID cuts, for two daughters of the D meson.

$$FoM = \frac{N_S}{\sqrt{N_S + N_B}} \tag{3.1}$$

$$\epsilon = \frac{N_S^{cut}}{N_S} \tag{3.2}$$

Here, N_S and N_B represent the numbers of correctly or incorrectly reconstructed candidates. The efficiency and figure of merit have maximum values when no further cut was applied, however the values did not drop rapidly with respect to the PID cut as shown in Figure 3-3 and 3-4. The results show that no further PID cut is essentially required after the preselection criteria. However in order to compare the result with that of the previous study, $L(K,\pi)_K > 0.6$ and $L(\pi,K)_\pi$

> 0.6 were chosen to be applied to every dataset. The efficiency regarding this cut were 0.85%, 0.89%, 0.91% and 0.9% for tagged $KK, \pi\pi, K\pi$ and untagged $K\pi$ modes, respectively.

3.3.2 Selection of Signal Window

Signal events are selected in the limited range around the nominal mass of the D^0. Thus the size of mass window should be determined to minimize the possible error from the window size. This uncertainty is approximated to the following equation, if the asymmetry is small enough.

$$\begin{aligned}
\sigma_A &= \frac{N^+ - N^-}{N^+ + N^-}\sqrt{(\frac{\sigma_{N^+-N^-}}{N^+ - N^-})^2 + (\frac{\sigma_{N^++N^-}}{N^+ + N^-})^2} \\
&= \frac{\epsilon}{N^+ + N^-}\sqrt{(\frac{\sigma_{N^++N^-}}{\epsilon})^2 + (\frac{\sigma_{N^++N^-}}{N^+ + N^-})^2} \\
&= \frac{1}{N^+ + N^-}\sqrt{\sigma^2_{N^++N^-}} \\
&= \frac{\sqrt{N_S + 2N_B}}{N_S}
\end{aligned} \tag{3.3}$$

From 3.3, the window size in each channel are optimized with the MC signal flag : where signal and background are discriminated by the signal flag. Thus, N_S and N_B correspond to the number of true particles selected with isSignal==1, and the number of entries with isSignal!=1. The results are shown in Figure 3-5. Final selection of signal window and estimated error are listed in Table 3-3.

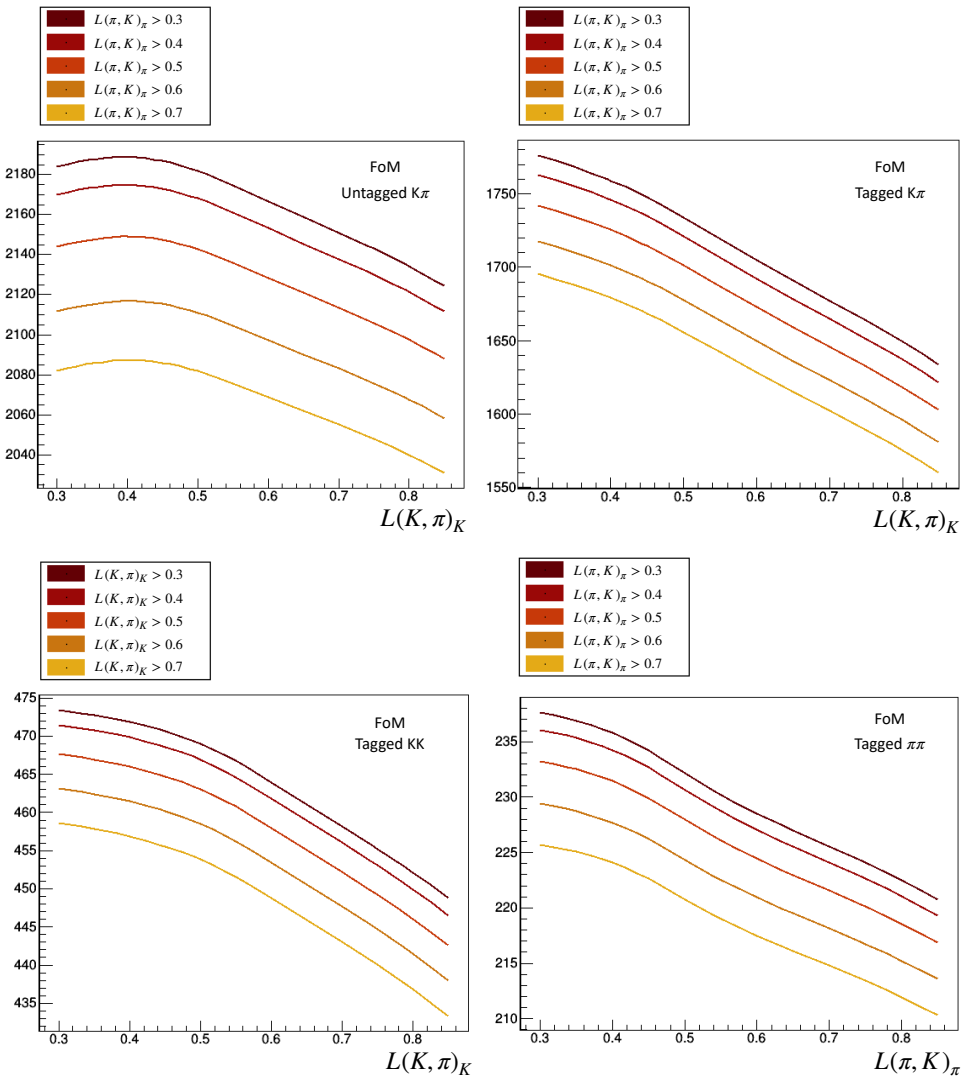

[Figure 3-3] FoM with respect to the binaryPID selection criteria

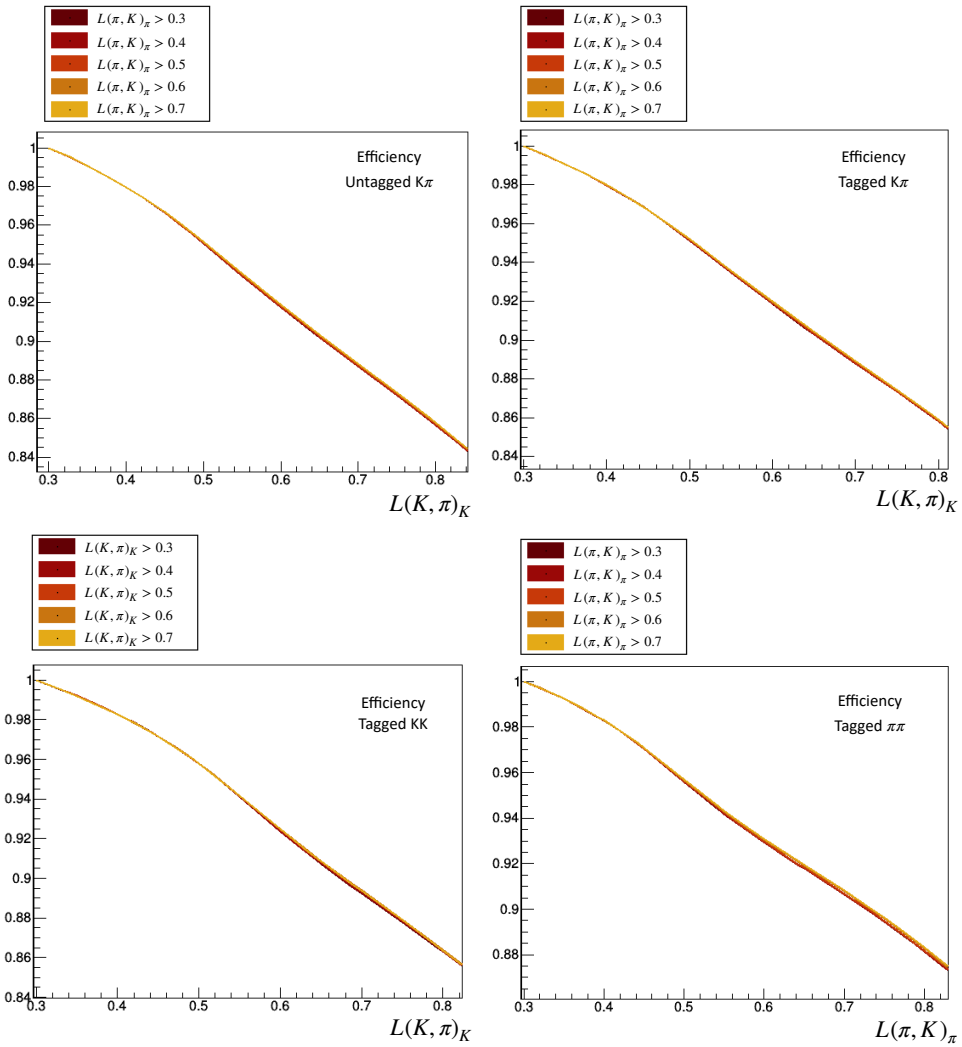

[Figure 3-4] efficiency with respect to the binaryPID selection criteria

[Table 3-3] Minimum estimated asymmetry regarding the width of signal window

	$D^0 \to K^+K^-$	$D^0 \to \pi^+\pi^-$	$D^0 \to K^-\pi^+$
M_{D^0}	0.017 GeV (0.224%)	0.015GeV (0.42 %)	0.015GeV (0.076%)
ΔM	0.0017GeV (0.21%)	0.0017GeV(0.38%)	0.002GeV(0.059%)

3.4 Yield Fit

The signal yield is obtained from simultaneous fits on $D^0$and $\overline{D}^0$ candidates. A large portion of background originates from combinatorial or misidentified final state particles; either one of the kaon or pion decaying from D^0 can be recognized as the other. The shape of these backgrounds can be easily discriminated from the signal; Restraining the mass range and applying a tight cut on PID criteria should be enough to suppress this background. Hence, only a mass fit is applied to the untagged channel. On the other hand, the tagged D^0 decays have another source of background originating from wrong slow pions. This background produces a narrow peak at theD^0 mass window but has a broad distribution along the ΔM distribution. Thus, the tagged decays require a 2-dimensional fit on mass andΔM. 2D histograms are firstly projected to each axis and fitted to pdf with minimum chi-square method in order to find an optimal parameters. Two models from each axis are combined together with two

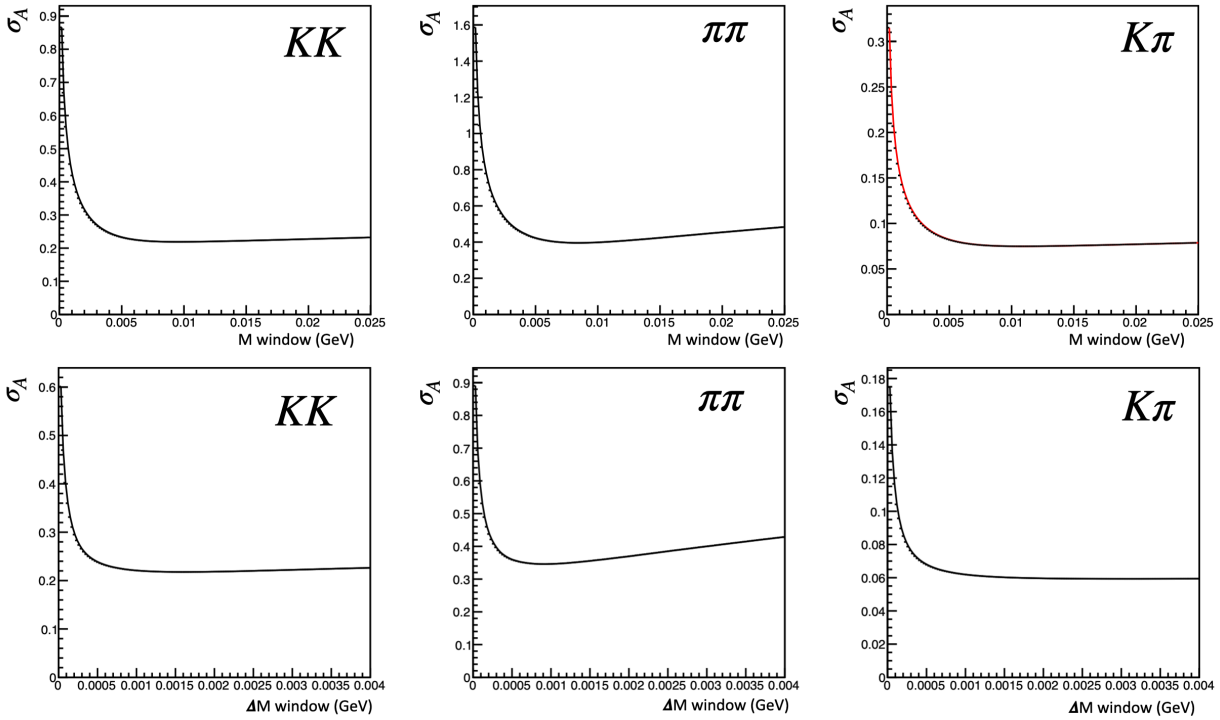

[Figure 3-5] Estimated asymmetry regarding the width of signal window. The selection criteria in Cabibbo favored channel should be consistent Thus the mass window of $D^0 \to K^-\pi^+$ is optimized the quadratic of their error[4]

floating parameters - signal and background yield. Other parameters are fixed. The signal and background models used for each channel are listed in below .

- Mass distribution
  - Signal ; Bifurcated Gaussian and a Gaussian with common mean
  - Physical background ; Gaussian with fixed mean(PDG value[2])
  - Combinatorial background first order polynomial
- ΔM distribution
  - Signal ;Johnson's SU distribution
  - Physical background ; A Bifurcated Gaussian
  - Combinatorial background; Threshold function[1]

Figure 3-7 and 3-6 present the fit results at the the projection on each axis. Resulting yields are provided in Table 3-4. Together with this result and the optimized sideband width, signal samples are selected from the signal distribution. The term D^0 candidate only represents the selected events from here.

[Table 3-4] Fit result

Decay Mode	N_{sig}	N_{bkg}
$D^0 \to K^+K^-$	$2.58 \times 10^5 \pm 5.28 \times 10^2$	$6.77 \times 10^4 \pm 2.97 \times 10^2$
$D^0 \to \pi^+\pi^-$	$1.30 \times 10^5 \pm 1.46 \times 10$	$1.72 \times 10^5 \pm 5.25$
$D^0 \to K^-\pi^+$	$3.02 \times 10^6 \pm 1.77 \times 10^3$	$1.34 \times 10^5 \pm 4.9 \times 10^2$
untagged $D^0 \to K^-\pi^+$	$7.93 \times 10^6 \pm 3.29 \times 10^3$	$5.88 \times 10^6 \pm 2.97 \times 10^3$

[1] RooDstD0 pdf defined in Roofit

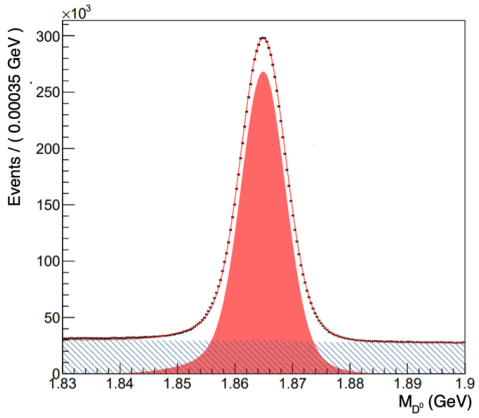

[Figure 3-6] Fit result of Untagged D^0 to $\pi^+\pi^-$ fit result

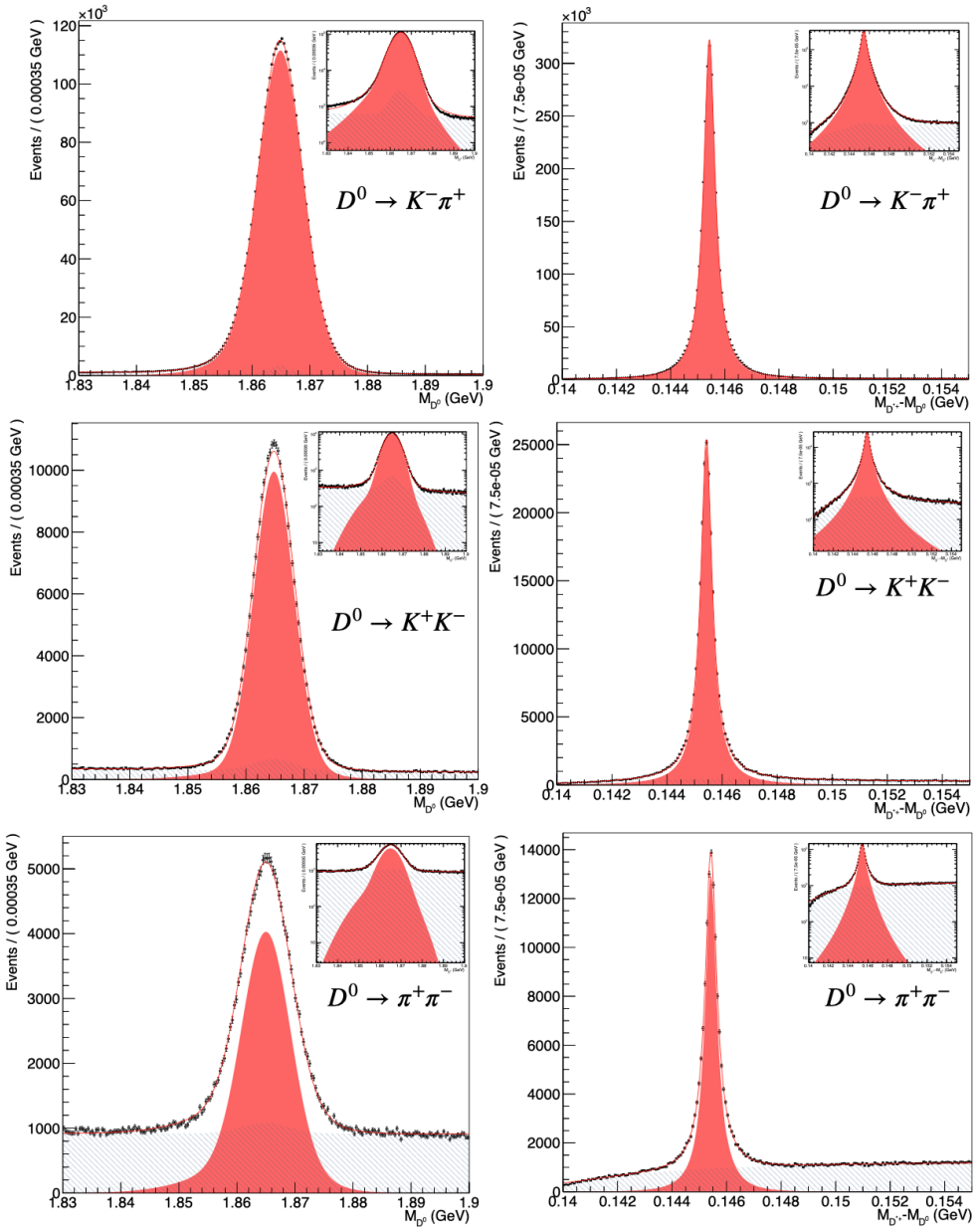

[Figure 3-7] Fit result of Tagged D^0 to $\pi^+\pi^-$ fit result. log scale plots are also shown in the top right in the each plots.

CHAPTER 4 ACP Measurement

4.1 D^0 raw asymmetry distribution

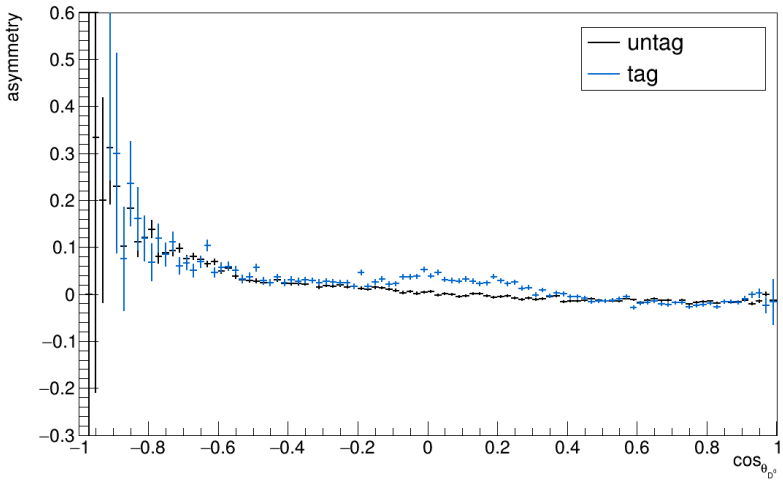

[Figure 4-1] The raw asymmetry of D^0 along $\cos\theta$

4-1 shows the raw asymmetry of D^0, along $\cos\theta$- The large asymmetries in the extreme forward and backward regions are considered to arise from slow pion's charge-dependent response in the detector material. Thus, D^0 candidates in the $\cos\theta > 0.9$ bin are rejected to avoid large statistical fluctuations. Additionally, an unanticipated difference appears at the center of the distribution due to the abnormally large asymmetry of the tagged channel in this region. This abnormal shape also appears in the asymmetry along with the momentum of D^0 , as depicted in Figure 4-2. Investigating the origin of this asymmetry is beyond the scope of this analysis. However, to verify that this asymmetry originates from

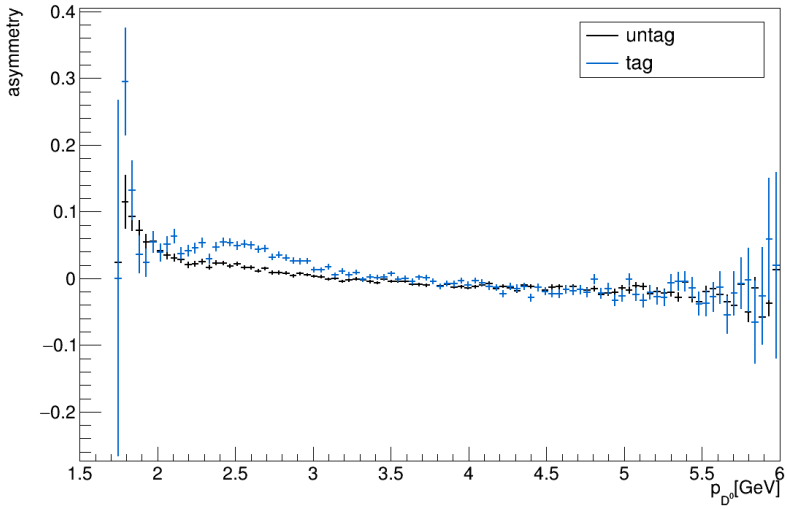

[Figure 4-2] The raw asymmetry of D^0 along p

the slow pion, the transverse momentum distributions of the slow pion in each tagged channel were inspected as shown in Figure 4-3.

A threshold at 0.25 GeV was observed in every tagged sample. As the amount of asymmetry was similar in every tagged sample, this abnormal asymmetry is expected to be neglected in the weighting procedure.

4.2 Raw Asymmetry and Slow Pion

The raw asymmetry A_{raw} of untagged D^0 is calculated in 20x20 bins of $\cos\theta$ and p space with Equation 4.1

$$A_{raw}^{untag}(p_{D^0}, \cos\theta_{D^0}) = \frac{N^+ - N^-}{N^+ + N^-} \tag{4.1}$$

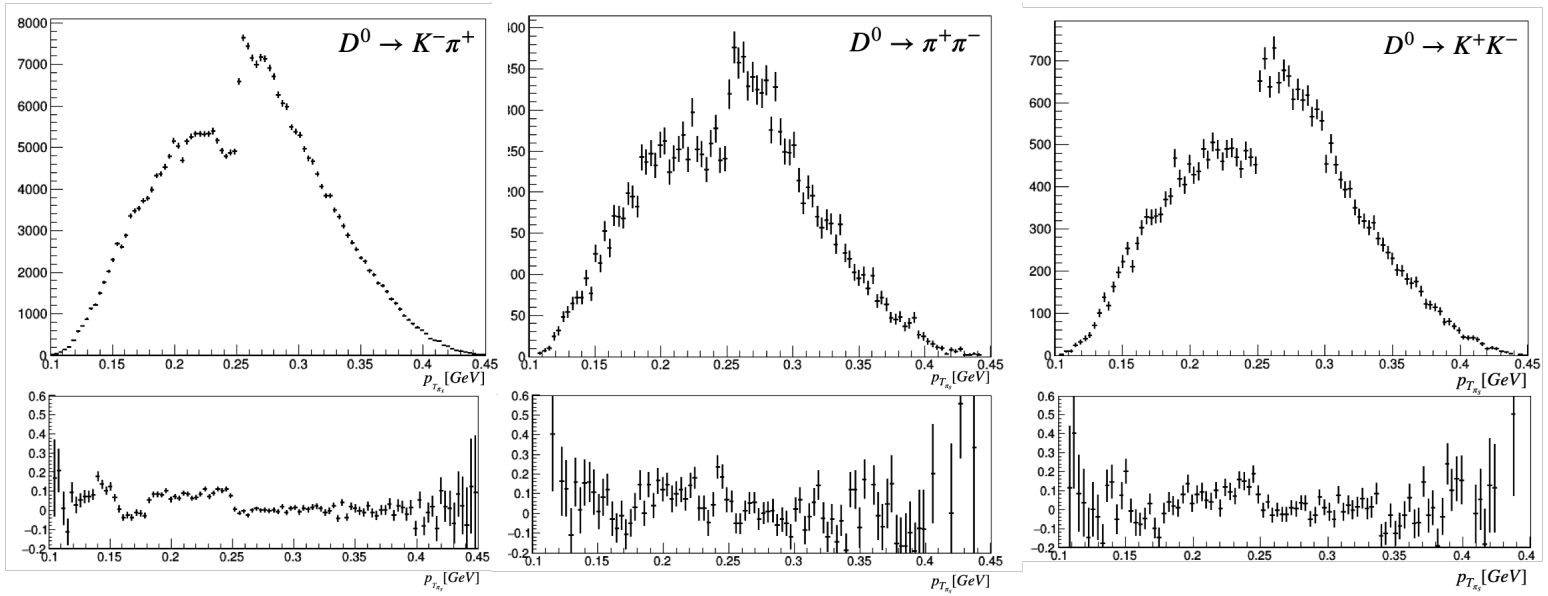

[Figure 4-3] slow pion transverse momentum distribution and asymmetry p

Here, N is the number of reconstructed D mesons, where + denotes the flavor; positive represents D^0 and - represents $\overline{D}^0$. During the calculation, bins with less than 1000 candidates are considered invalid to minimize the statistical error. The resulting asymmetry is presented in 4-5.

Tagged Kπ events corresponds to valid bins of A_{raw}^{untag} are weighted as in 4.2.

$$\begin{aligned} w_{D^0} &= 1 - A_{raw}^{untag}(p_{D^0}, \cos\theta_{D^0}) \\ w_{\overline{D}^0} &= 1 + A_{raw}^{untag}(p_{\overline{D}^0}, \cos\theta_{\overline{D}^0}) \end{aligned} \tag{4.2}$$

A_{ϵ}^{π} is calculated in terms of the pion's momentum, and the polar angle bin is defined as shown in 4.3. n is the sum of the weight of the D mesons in the bin. The corrected asymmetry of $D^0 \to K^+K^-$ and $D^0 \to \pi^+\pi^-$ are binned along $|\cos\theta^*|$. Events with $|\cos\theta^*| < 0.8$ are selected since the momentum cut restricts the CMS momentum to that region.

$$A_{\epsilon}^{\pi_s}(p_{\pi_s}, \cos\theta_{\pi_s}) = \frac{\Sigma w_{D^0}(p_{\pi_s}, cos\theta_{\pi_s}) - \Sigma w_{\overline{D}^0}(p_{\pi_s}, \cos\theta_{\pi_s})}{\Sigma w_{D^0}(p_{\pi_s}, \cos\theta_{\pi_s}) + \Sigma w_{\overline{D}^0}(p_{\pi_s}, \cos\theta_{\pi_s})} \tag{4.3}$$

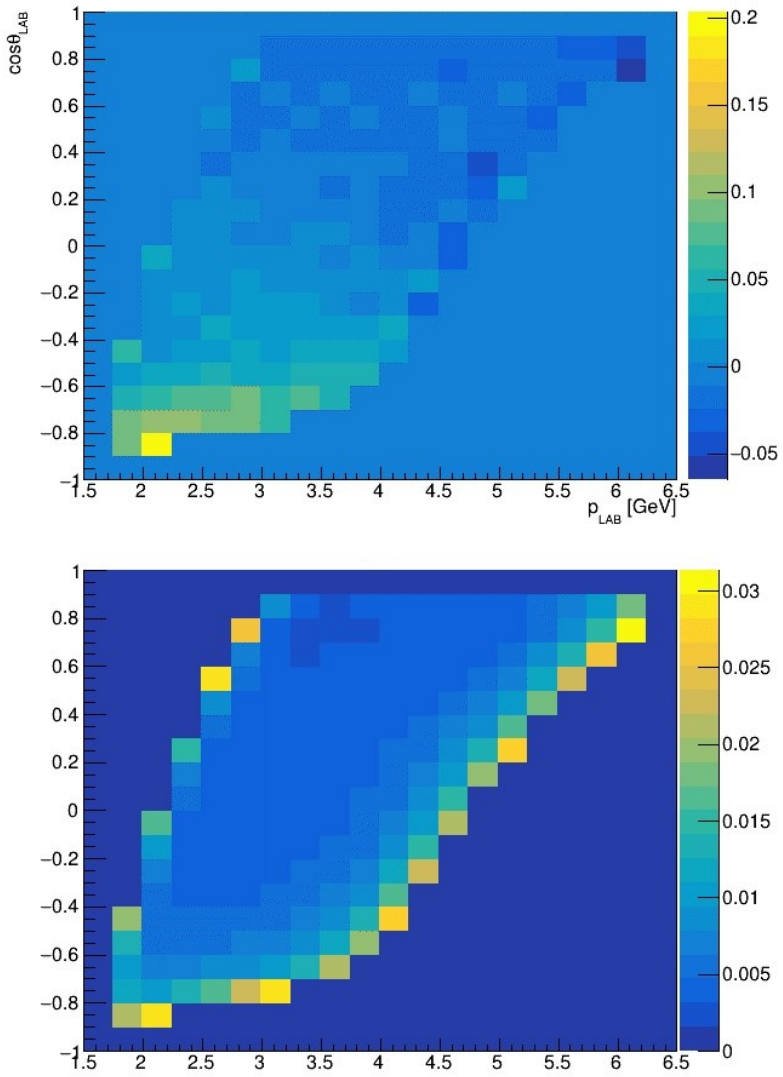

[Figure 4-4] A_{raw}^{untag} (above) and corresponding statistical error (below)

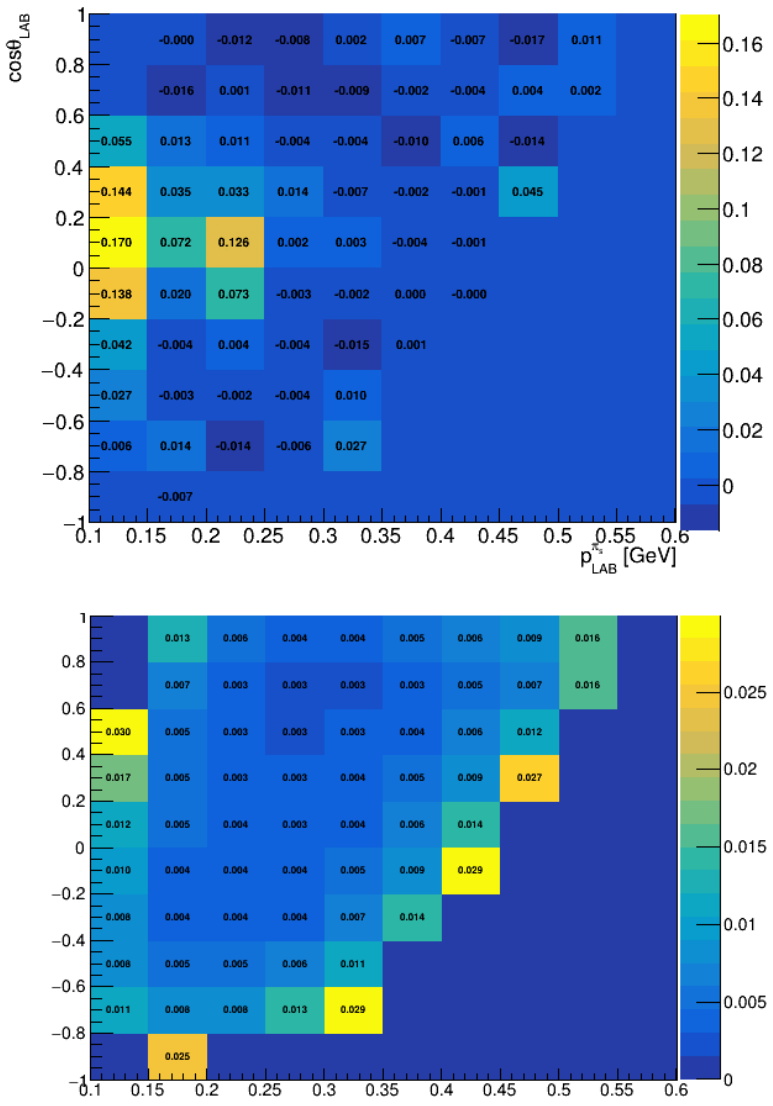

[Figure 4-5] A_{ϵ}^{π} (above) and statistical error (below)

4.3 Linear fit of A_{CP}

The obtained value of $A_\epsilon^{\pi_s}$ is finally used to correct singly Cabibbo suppressed channels by weighting each $D^0, \overline{D}^0$ candidate using 4.4. The corrected asymmetry is expressed in Equation 4.5.

$$\begin{aligned} u_{D^0} &= 1 - A_\epsilon^{\pi}(p_{\pi_s}, \cos\theta_{\pi_s}) \\ u_{\overline{D}^0} &= 1 + A_\epsilon^{\pi}(p_{\pi_s}, \cos\theta_{\pi_s}) \end{aligned} \tag{4.4}$$

$$A_{corr}^{hh,rec}(cos\theta^*) = \frac{\Sigma u_{D^0}(cos\theta^*) + \Sigma u_{\overline{D}^0}(cos\theta^*)}{\Sigma u_{D^0}(cos\theta^*) + \Sigma u_{\overline{D}^0}(cos\theta^*)} \tag{4.5}$$

Finally, A_{CP} and A_{FB} are calculated 8 bins in $|\cos\theta^*| < 0.8$ region using Equation 1.4 and fitted with constant function which has single parameter. The chi-square minimization method was employed for fitting. Fit results are presented in Figure 4-7 and 4-6 where the fit result and the 68% confidence interval of the fit are indicated in the blue line and the yellow boxes. The error only includes statistical errors. The results and statistical errors are: A_{CP}^{KK} = -0.0004562 ± 0.002068 and $A_{CP}^{\pi\pi}$ = 0.0005645 ± 0.0031997.

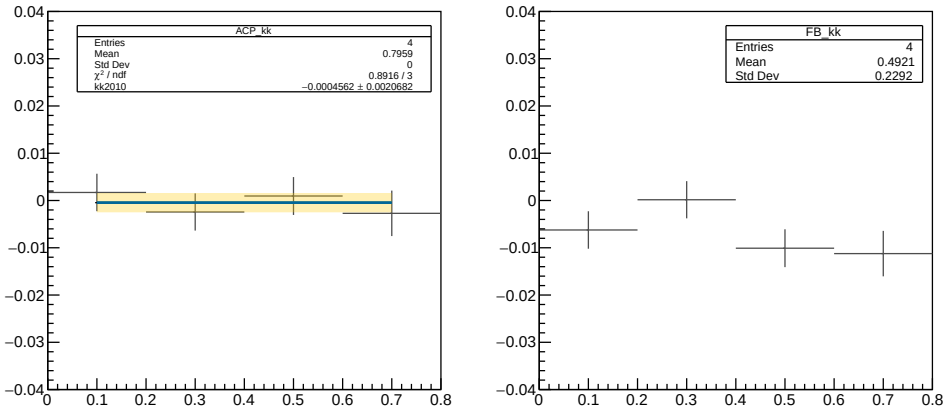

[Figure 4-6] A_{CP}^{KK} (left) and statistical A_{FB}^{KK} (right)

4.4 Systematic

Systematic errors can occur in the following steps throughout the analysis; (1) The shape difference between D^0 and $\overline{D}^0$ and (2) the signal and sideband can be considered in the signal counting. (3) The number of the bin of the asymmetry map, and(4) Bin numbers along the $|\cos\theta^*_{D^{*+}}|$ should also be considered in the $A_\epsilon^p i$ extraction. In this analysis, only (3) and (4) are investigated from the outset since the asymmetry distribution has an irregular shape, as discussed in section 4.1.

- The number of the bin of the asymmetry map

  A_{CP} results from 9 different bin combinations of maps; 10x10,20x20, 50x50 bins for $A_{raw}$and 5x5, 10x10, 20x20 for $A_\epsilon^{\pi_s}$ are compared. The

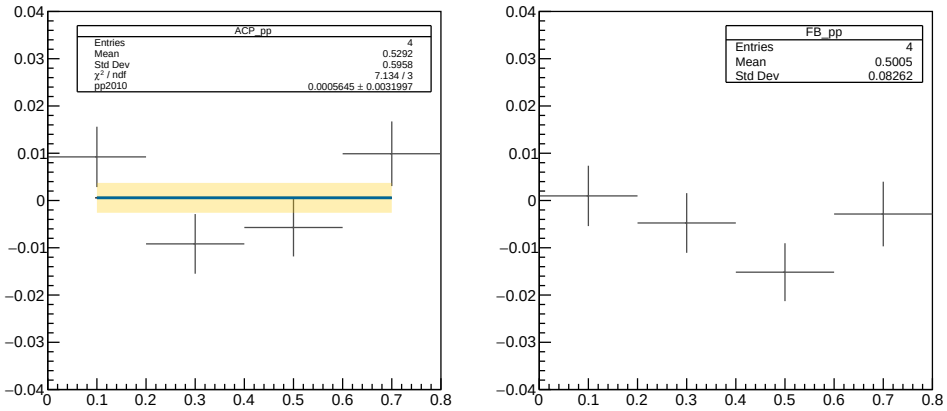

[Figure 4-7] $A_{CP}^{\pi\pi}$ (left) and statistical $A_{FB}^{\pi\pi}$ (right)

standard deviation is 0.006% for the KK channel, 0.014% for the $\pi\pi$ channel and 0.010% for the A_{CP} calculation.

- Bin numbers along the $|\cos\theta_{D^{*+}}^{*}|$

  A_{CP} results from 8,16,32,64 bins along $\cos\theta_{D^{*+}}^{*}$ are compared. Largest difference among the results was 0.007% for KK samples, and 0.005% for $\pi\pi$ samples. 0.0069% deviation was calculated in ΔA_{CP}

Quadratic sum of each samples are 0.0092 for KK, and 0.025 for $\pi\pi$ and 0.012.

CHAPTER 5 Conclusion

[Table 5-1] Result

A_{CP}^{KK}	(-0.046 ± 0.21 ± 0.01)%
$A_{CP}^{\pi\pi}$	(0.056 ± 0.32 ± 0.025)%
$A_{CP}^{KK} - A_{CP}^{\pi\pi}$	(-0.10 ± 0.38 ± 0.012)%

This study employed the D^{*+} tagging method to calculate the amount of direct CPV in the $D^0 \to K^+K^-$ and $D^0 \to \pi^+\pi^-$ decays using 1/ab of Belle II Monte Carlo data. The fit results, statistical uncertainties, and partial systematic uncertainties are summarized in Table 5-1. Considering the fact that the fit value is consistent with zero, a value initially set in the simulation data sample, and the statistical uncertainties correspond well to those shown in the previous Belle study[4], the validity of the analysis method is again confirmed. We are planning to use this analysis method for a further study on collision data samples produced by Belle II. The amount of statistical errors are expected to be decreased by farcof of 7, if BelleII collect 50/ab until the end of its run.

Future studies on this subject should be focused on in-depth analysis on systematic uncertainties: the possible sources of systematic uncertainties were already discussed in 4.4, but the results shown in the table of this Chapter only included the systematic uncertainty coming from the number of histogram bins at the phase space of D^0 and π_ϵ momentum and polar angle. The investiga-

tion on the discontinuous shape of slow pion momentum distribution needs to be undertaken to understand its origin and effect on the D^{*+} tagging method.

REFERENCES

[1] F and others Buccella. “Nonleptonic weak decays of charmed mesons”. *Physical Review D* 51.7 (1995). Publisher: APS, page 3478.

[2] P.A. Zyla *et al.* “Review of Particle Physics”. *PTEP* 2020.8 (2020), page 083C01.

[3] J. P. Lees *et al.* “Search for direct CP violation in singly Cabibbo-suppressed $D^{\pm} \to K^{+}K^{-}\pi^{\pm}$decays”. *Physical Review D* 87.5 (2013). Publisher: American Physical Society (APS).

[4] M. Staric. “Measurement of CP asymmetry in Cabibbo suppressed D0 decays”. *Physics Letters B* 670.3 (2008), pages 190–195.

[5] R. Aaij *et al.* “Observation of CP Violation in Charm Decays”. *Phys. Rev. Lett.* 122 (21 2019), page 211803.

[6] Kazunori Akai, Kazuro Furukawa and Haruyo Koiso. “SuperKEKB collider”. *Nuclear Instruments and Methods in Physics Research Section A: Accelerators, Spectrometers, Detectors and Associated Equipment* 907 (2018). Publisher: Elsevier BV, pages 188–199.

[7] SuperB Collaboration. *SuperB: A High-Luminosity Asymmetric e+ e- Super Flavor Factory. Conceptual Design Report*. _eprint: 0709.0451. 2007.

[8] Chang-Zheng Yuan. “The Belle II Experiment at the SuperKEKB”. *EPJ Web of Conferences* 218 (2019). By editor A. Denig and C.-F. Redmer, page 07003.

[9] Belle2 Collaboration. “Belle II Technical Design Report”. *arXiv:1011.0352 [hep-ex, physics:physics]* (2010).

[10] I. Adachi *et al.* “Detectors for extreme luminosity: Belle II”. *Nuclear Instruments and Methods in Physics Research Section A: Accelerators, Spectrometers, Detectors and Associated Equipment* 907 (2018), pages 46–59.

[11] C Marinas. “The Belle II DEPFET vertex detector: current status and future plans”. *Journal of Instrumentation* 7.2 (2012), pages C02029–C02029.

[12] M. Friedl *et al.* “The Belle II Silicon Vertex Detector”. *Physics Procedia* 37 (2012), pages 867–873.

[13] N. Taniguchi. “Central Drift Chamber for Belle-II”. *Journal of Instrumentation* 12.6 (2017), pages C06014–C06014.

[14] S. Sandilya. “Particle Identification at Belle II”. *Journal of Physics: Conference Series* 770 (2016), page 012045.

[15] R. Pestotnik *et al.* “The aerogel Ring Imaging Cherenkov system at the Belle II spectrometer”. *Nuclear Instruments and Methods in Physics Re-*

search Section A: Accelerators, Spectrometers, Detectors and Associated Equipment 876 (2017), pages 265–268.

[16] J. Fast. “The Belle II imaging Time-of-Propagation (iTOP) detector”. *Nuclear Instruments and Methods in Physics Research Section A: Accelerators, Spectrometers, Detectors and Associated Equipment* 876 (2017), pages 145–148.

[17] Belle-ECL *et al.* “Electromagnetic calorimeter for Belle II”. *Journal of Physics: Conference Series* 587 (2015), page 012045.

[18] T. Aushev *et al.* “A scintillator based muon and KLong detector for the Belle II experiment”. *Nuclear Instruments and Methods in Physics Research Section A: Accelerators, Spectrometers, Detectors and Associated Equipment* 789 (2015), pages 134–142.

[19] Doris Yangsoo Kim. “Software and Physics Simulation at Belle II”. (), page 6.

[20] S. Agostinelli *et al.* “Geant4—a simulation toolkit”. *Nuclear Instruments and Methods in Physics Research Section A: Accelerators, Spectrometers, Detectors and Associated Equipment* 506.3 (2003), pages 250–303.

[21] Swagato Banerjee *et al.* “Optimization of Geant4 for the Belle II software library”. *EPJ Web of Conferences* 251 (2021). By editor C. Biscarat *et al.*, page 03024.

[22] Leo Piilonen. “Belle II VR: A Virtual Reality Visualization of Subatomic Particle Physics”. (2018).

[23] Z. Duer, L. Piilonen and G. Glasson. “Belle2VR: A Virtual-Reality Visualization of Subatomic Particle Physics in the Belle II Experiment”. *IEEE Computer Graphics and Applications* 38.3 (2018). Place: Los Alamitos, CA, USA Publisher: IEEE Computer Society, pages 33–43.

[24] Silvio Pardi, Guglielmo de Nardo and Guido Russo. “Computing at Belle II”. *Nucl. Part. Phys. Proc.* 273-275 (2016), pages 950–956.

[25] F Stagni *et al.* “DIRAC in Large Particle Physics Experiments”. *Journal of Physics: Conference Series* 898 (2017), page 092020.

[26] Matthew Barrett *et al.* “The Belle II Online–Offline Data Operations System”. *Computing and Software for Big Science* 5.1 (2021), page 1.

[27] David M. Asner, Eli Dart and Takanori Hara. *Belle II Experiment Network and Computing*. 2013. arXiv: 1308.0672 [physics.ins-det].

[28] Martin Sevior, Tom Fifield and Nobuhiko Katayama. “Belle monte-carlo production on the Amazon EC2 cloud”. *Journal of Physics: Conference Series* 219.1 (2010), page 012003.

[29] T. Kuhr *et al.* “The Belle II Core Software”. *Computing and Software for Big Science* 3.1 (2018).